https://doi.org/10.5194/egusphere-2026-1135
Preprint. Discussion started: 17 March 2026

Multi-sensor satellite analysis reveals latitudinal and morphometric controls on ice phenology across 31,000 thermokarst lakes on the Alaska North Slope

Alexander L. Nguyen[1*], Cesar G. Lopez[1*], Jennifer Melara-Valle[1], Eliza Ross[1], Alexander S. Bradley[1], Maggie R. Limbeck[1], Claire C. Masteller[1], Roger Michaelides[1]

[1]Department of Earth, Environmental, and Planetary Sciences, Washington University in St. Louis, Saint Louis, MO, 63130, USA
* These authors contributed equally to this work

Correspondence to: Roger Michaelides (roger.michaelides@wustl.edu)

Abstract. Thermokarst lakes are critical components of Arctic carbon cycling, yet their ice phenology, which directly impacts total carbon flux, remains poorly characterized at regional scales. We present the first comprehensive analysis of ice-on and ice-off timing across 30,862 lakes on the Alaska North Slope using Sentinel-1 synthetic aperture radar (SAR) classified by a Random Forest (RF) model trained on Sentinel-2 optical imagery and ERA5 temperature data for the period 2019–2023. Our RF classifier achieved 94% accuracy for ice state detection, enabling phenology retrieval for 97% of lakes. Results revealed a mean ice-free period of 115 days (standard deviation = 24 days), with ice-off occurring at day-of-year 163 (June 12) and ice-on at day-of-year 278 (October 5). Spatial analysis demonstrated strong latitudinal control on ice phenology, with ice-free duration decreasing by 30 days per degree northward. Lake morphology (area, circularity, convexity, and shoreline development index) showed modest but significant effects on ice timing after controlling for latitude effects, with shoreline development index and convexity each contributing ~three days variation across typical lake ranges. Comparison of the RF model and simplistic accumulated degree-day (ADD) model-detected ice phenology yielded a convincing match, where the offsets in ice phenology between the models fell within two Sentinel-1 repeats for approximately 60% of the lakes. Furthermore, these offsets exhibited the same strong latitudinal control and negligible effects of lake morphology. These lake-specific phenology dates provide timing and duration constraints for future methane studies using high-resolution sensors and provide baseline phenology data essential for understanding how continued Arctic warming will affect thermokarst lake dynamics and associated carbon cycle feedbacks.

1 Introduction

The Arctic is warming at nearly two to four times the global average rate (Rantanen et al., 2022), with profound implications for thaw on permafrost landscapes. This Arctic Amplification (Serreze and Barry, 2011) impacts Arctic landscapes through processes such as the permafrost carbon feedback (Schurr et al., 2015), alteration of surface hydrology (Lafrenière and Lamoureux, 2019), and ground subsidence (Streletskiy et al., 2025). Formed by ground subsidence following permafrost thaw,

https://doi.org/10.5194/egusphere-2026-1135
Preprint. Discussion started: 17 March 2026

thermokarst lakes cover more than 20% of the Alaskan Arctic Coastal Plain (Arp et al., 2011) and approximately 17% of Arctic lowland terrain globally (Muster et al., 2017).

Thermokarst lakes represent dynamic components of high-latitude carbon cycling, where permafrost thaw surrounding these lakes mobilizes stored soil organic material (In 'T Zandt et al., 2020). These lakes emit substantial quantities of methane (CH_4) and carbon dioxide (CO_2) to the atmosphere (Walter Anthony et al., 2018), where current estimates for yearly CH_4 emissions from thermokarst lakes larger than 0.1 km^2 are 24.0 ± 8.4 Tg CH_4 yr^{-1} (Zhuang et al., 2023). Emissions are strongly modulated by lake area and depth (Heslop et al. 2020; Manasypov et al., 2023; Matthews et al., 2020; West et al. 2015) and the duration of ice melt and seasonal ice cover (Mu et al., 2025; Wik et al., 2016; Guo et al., 2020). However, the influence of lake morphometrics on ice condition and timing (i.e., duration of ice melt and seasonal ice cover) is relatively understudied.

Ice phenology - the timing of ice formation (ice-on) and breakup (ice-off) - controls the duration of open-water conditions during which gas exchange with the atmosphere occurs. Despite the importance of ice timing for understanding carbon fluxes, comprehensive regional-scale phenology data remain scarce at high spatiotemporal resolution (< 0.25 km/pixel/week) (Matthews et al., 2020). Previous studies have either focused on direct observation of ice phenology for individual lakes using *in situ* observations (Arp et al., 2015) or use single-sensor/single-modality satellite approaches for lake populations with a relatively limited number of lakes (< 1000; Latifovic and Pouliot, 2007; Surdu et al., 2014, 2016; Tom et al., 2020). The challenge of monitoring hundreds of thousands of thermokarst lakes across the remote Arctic terrain, combined with persistent cloud cover and polar night conditions, has hindered systematic phenology characterization. This technical challenge limits our ability to resolve the timing and duration of freeze-thaw transitions and detect climate-driven shifts in ice phenology, constraining efforts to quantify lake-atmosphere carbon exchange and accurately represent thermokarst lake processes in regional and global Earth system models.

Current direct methods for determining lake ice phenology are often based on ice thickness estimates, which typically utilize simplistic thermal diffusion metrics such as the modified Stefan equation for accumulating degree days (ADD) (ºC · d; Arp et al., 2015; Stefan, 1890). ADD metrics are determined from air temperature records and do not account for lake-specific morphology (USACE, 2004). More complex models may incorporate lake depth, which captures ice thickness, but do not generally account for other morphologic parameters such as area, circularity, convexity, or shoreline properties, as these features are difficult to estimate without *in situ* measurements (Duguay et al., 2003). As a result, the degree to which thermokarst lake morphology may influence ice phenology relative to estimates based on ADD metrics remains largely unknown. Previous studies suggest that lake morphology, especially area and depth, play an important role in modulating ice phenology (Basu et al., 2024; Higgins et al., 2021; Smits et al., 2021). However, these studies do not pertain or are not exclusive to Arctic thermokarst lakes. To our knowledge, no comprehensive study on the role of thermokarst lake morphology in controlling ice phenology exists at the regional scale.

Recent advances in satellite remote sensing offer new opportunities for large-scale ice monitoring (Bartsch et al. 2023). The Sentinel-1 synthetic aperture radar (SAR) operates independently of solar illumination and cloud cover, providing year-round observations at ~10-20 m spatial resolution. The distinct microwave radar backscatter signatures of ice versus open water

https://doi.org/10.5194/egusphere-2026-1135
Preprint. Discussion started: 17 March 2026

enable automated ice detection for thermokarst lakes (Bartsch et al., 2017; Tom et al. 2020), though interpretation can be complicated by factors including ice thickness and structure, snow cover, bulk water content, and surface roughness that all impact radar scattering properties (Hall et al., 1994; Jeffries et al., 1994). However, Sentinel-2 optical imagery provides complementary information through spectral indices such as the Normalized Difference Snow Index (NDSI), which discriminates ice from water under sun-lit, clear-sky conditions (Riggs et al., 2016). NDSI can aid in SAR interpretation and fill in dates within the Sentinel-1 6 day repeat time when using both polar orbiting ascending and descending tracks. By combining these observations with temperature data from atmospheric reanalysis products, robust ice classification can be achieved across the full annual cycle, allowing for a regional-scale exploration of the morphologic controls on lake ice phenology.

In this contribution, we present a multi-sensor fusion approach to characterize ice phenology and its relationship to morphological parameters across 30,862 thermokarst lakes on the Alaska North Slope. Our objectives are to: (1) develop and validate an automated ice detection algorithm combining SAR, optical, and temperature data; (2) quantify spatiotemporal patterns in ice-on and ice-off timing across the study region relative to ADD-predicted timing; (3) examine relationships between lake morphometry and ice phenology. This analysis provides the most comprehensive characterization of regional-scale thermokarst lake ice phenology to date, establishing baseline conditions against which future changes can be assessed.

2 Methods

2.1 Study area and lake dataset

The study area encompasses the Arctic Coastal Plain (ACP) of the North Slope of Alaska (~69 °N - 71.36 °N), a ~200,000 km^2 region of continuous permafrost extending from the Brooks Range foothills to the Arctic Ocean (Fig. 1). This low-relief coastal plain is characterized by hundreds of thousands of 2 – 4 meter deep thermokarst lakes formed in ice-rich permafrost deposits (Hinkel et al. 2012). The region experiences a polar climate with mean annual temperatures of -10 to -12 °C, though summer temperatures regularly exceed 15 °C.

We obtained lake boundaries from the Alaska Lake and Pond Occurrence Dataset (ALPOD; Levenson et al., 2025), which provides high-resolution (10 m/pixel) lake polygons derived from a U-Net lake detection model (Mullen et al. 2023) applied to multi-temporal Sentinel-2 imagery across Alaska that totals in 801,895 lakes. The selected study region (69 °N - 71.36 °N, 163.85 °W - 141.02 °W) contains 128,197 ALPOD lakes. We selected all lakes ≥ 0.02 km² (2 ha) to ensure each lake had a large enough number of pixels (200 for 10 m/pixel imagery) for reliable Sentinel-1/2 detection. This selection yielded 31,108 total lakes total for analysis, which encompasses the upper ~25th percentile of lake area distribution prior to area filtering (Fig. S19). From this, we were able to retrieve phenology from 30,862 lakes (99.2%), where lake morphometrics could be extracted using lake polygons from the ALPOD database.

For the subpopulation of lakes used in this study, lake area spans five orders of magnitude from 0.02 to 859 km² (median = 0.065 km²), with the upper bound corresponding to Teshekpuk Lake. Study lakes had a range of circularity, defined as C =

https://doi.org/10.5194/egusphere-2026-1135
Preprint. Discussion started: 17 March 2026

$4\pi A/P^2$, where P is lake perimeter (m), from 0.01 – 0.78, with smaller values indicative of more oblong lakes. Lake shoreline development indices, (SDI = $P/2\sqrt{\pi A}$; Hutchinson, 1957), which quantifies shoreline complexity, range from 1.13 – 10.02, with larger values indicating more complex shorelines. Measures of lake convexity range from 0.11 - 0.998, where values of 1.0 indicate more convex shorelines and values closer to zero signify higher concavity or shoreline irregularity (Bozeman and Pilling, 2013). Calculating both SDI and convexity allows for a better understanding of both shoreline complexity and irregularity, where SDI is more impacted by fractal dimensionality from higher resolution data and increases with increasing area of lakes (Seekell et al. 2022). Lake circularity, SDI, and convexity for the subpopulation of lakes used in this study were consistent with metrics from the full ALPOD database (Fig. S19).

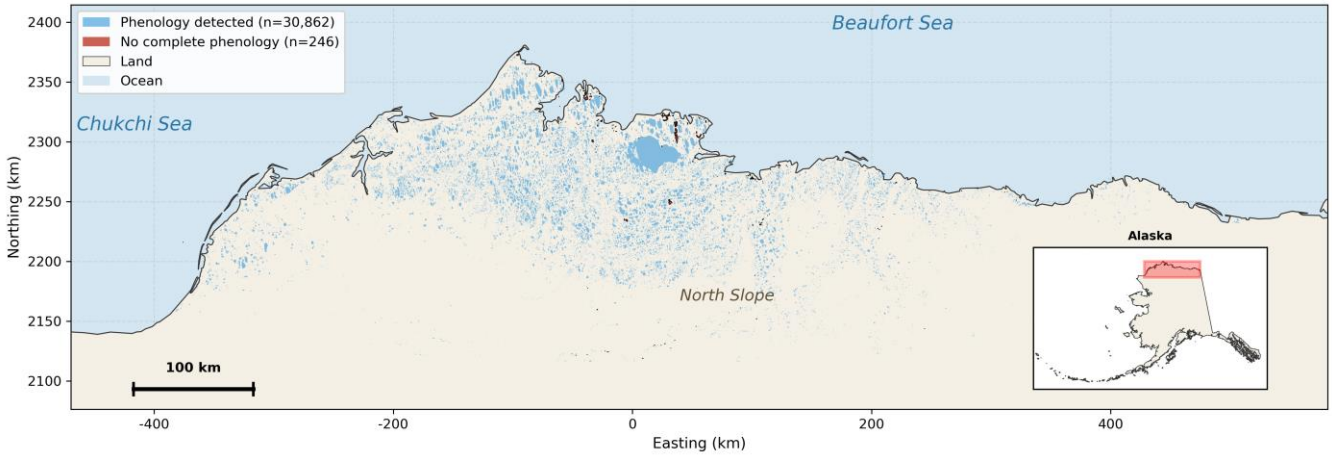

Figure 1: Study area (69 °N - 71.36 °N, 163.85 °W - 141.02 °W) showing the total 31,108 lakes, and 30,862 lakes with area ≥ 0.02 km^2 (blue) on the Alaska North Slope in the ALPOD dataset in which phenology was detected. Lakes in which phenology was not successfully detected are shown in bronze. Inset depicts mapped location within Alaska. Sources: ALPOD and the Natural Earth.

2.2 Satellite data acquisition and preprocessing

We acquired Sentinel-1 Ground Range Detected (GRD) imagery from Google Earth Engine (GEE) (Gorelick et al., 2017) for the period January 2019 through December 2023. We used images from both ascending and descending track satellite orbits acquired in Interferometric Wide Swath mode, providing both vertical transmit/receive (VV) and vertical transmit/horizontal receive (VH) polarizations at 10 m resolution. Images were accessed from the GEE Sentinel-1 GRD collection, which provides data pre-processed using the standard Sentinel-1 Toolbox workflow including thermal noise removal, radiometric calibration, and orthorectification terrain correction (Mullissa et al., 2021). We additionally applied an incidence angle mask (25–50°) to reduce edge effects, and we subtracted VH from VV images to generate VV/VH images. We generated standard false-color RGB composites of backscatter (i.e., red: VV, green: VH, blue: VV/VH). To account for typical Arctic lake backscatter

https://doi.org/10.5194/egusphere-2026-1135
Preprint. Discussion started: 17 March 2026

ranges, we scaled each band (in order) for open water to rough ice (-20 to –5 dB; VV), volumetric scattering cross-polarization range (-28 to –12 dB; VH), and the polarization ratio (8 to 18 dB; VV/VH).

We obtained Sentinel-2 Level-2A surface reflectance imagery for the same time period between 2019 – 2023, where our study period date range is limited by Sentinel-2 Level-2A products being unavailable for 2017-2018. We then filtered to acquisitions with <80% scene cloud cover and pixel-level cloud and cloud shadow masking using the s2cloudless algorithm with a 20% cloud probability threshold (Sentinel-Hub, 2025; Skakun et al., 2022). Sentinel-2 coverage varies spatially across the study area due to orbital geometry at ~70 °N, with reduced coverage between –153 °W and –157 °W longitude; consequently, S2 observations serve as high-confidence training labels where available rather than as the primary detection method. We calculated the Normalized Difference Snow Index (NDSI) as NDSI = (Green − SWIR) / (Green + SWIR) using bands B3 (560 nm) and B11 (1610 nm) (Hall et al. 1995), and we classified NDSI values > 0.4 as snow/ice following established thresholds (Riggs et al., 2016).

We obtained ERA5 hourly 2 m air temperature data at 0.25° (~28 km/pixel) resolution from the Google Cloud Analysis-Ready, Cloud-Optimized (ARCO) ERA5 archive (Carver and Merose, 2023; Herbach et al. 2017; Hersbach et al., 2020) and aggregated to daily means for each lake centroid location.

2.3 Ice detection algorithm

Our ice detection approach uses a Random Forest (RF) classifier (Breiman, 2001) to predict ice state from Sentinel-1 SAR backscatter features. This approach follows machine learning methods developed for lake ice classification from SAR imagery (Hoekstra et al., 2020; Tom et al., 2020), adapted for regional-scale application. We derived training labels from two sources: ERA5 temperature reanalysis and Sentinel-2 optical imagery. Sustained temperature periods (10+ consecutive days below −20°C or above +10°C) provided high-confidence labels during winter months and polar night when optical data were unavailable, comprising approximately 62% of training labels. Sentinel-2 NDSI classifications provided the remaining labels during cloud-free conditions (30% cloud threshold), with temperature-based quality control to exclude potentially erroneous detections (e.g., S2 labels flagged as water when air temperature was below −5°C, or as ice when temperature exceeded +5°C, were excluded to filter algal bloom misclassifications). This dual-source approach maximizes temporal coverage across the full annual cycle while maintaining label reliability.

We trained the RF model on six Sentinel-1-derived features: VV and VH backscatter (dB) measured over the lake interior (extracted from removing a 10 m interior buffer applied to each lake feature perimeter), VV and VH backscatter over a 100 m marginal landscape surrounding each lake (extracted from adding a 100 m exterior buffer applied to each lake feature perimeter), and the VV/VH polarization ratio for both lake and landscape zones. High values of VV co-polarization record rough ice, whereas low values record smooth ice and water. VH cross-polarization is sensitive to volumetric scattering from vegetation, and the ratio between co- and cross-polarizations aids in determination between types of ice. Furthermore, the landscape features encapsulated through the exterior buffer capture contextual information about surrounding terrain conditions that may aid in distinguishing ice from open water (e.g., freeze/thaw state of the landscape).

https://doi.org/10.5194/egusphere-2026-1135
Preprint. Discussion started: 17 March 2026

Training data comprised 1.09 million lake-date observations from 24,886 lakes. An additional 274,079 observations from 6,222 held-out (validation) lakes were reserved for testing. This lake-based splitting strategy, implemented using grouped cross-validation, ensures no lake appears in both training and test sets, preventing data leakage from temporal autocorrelation within individual lake time series. We implemented the RF model using scikit-learn (Pedregosa et al., 2011) with 100 trees, a maximum depth of 15, a minimum split of 20 samples, and a minimum of 10 samples for leaves.

The RF classifier achieved 94% overall accuracy when evaluated against Sentinel-2 NDSI labels from the held-out/validation lakes not used in training (n = 106,527 observations from 2,322 lakes). Performance was higher for the ice class (precision = 0.97 recall = 0.95) than the water class (precision = 0.86, recall = 0.93), reflecting both the class imbalance in training data (65% ice, 35% water owing to the shorter ice-free season) and the greater difficulty of detecting open water conditions (Fig. S1). Cross-validated F1 score was 0.977 ± 0.001 Feature importance for the RF model was consistently higher for the land buffers surrounding the lakes for VH (green), VV (red), and VV/VH ratio (blue), respectively, compared to the lake interiors (VV, VH, and VV/VH ratio), which may indicate true importance or potential bias in the number of pixels used in the land vs lake buffers (Fig. S2). Accuracy estimates reflect agreement with optical classifications; no independent validation against field observations was performed. During inference, ice state is determined solely by the RF classifier applied to Sentinel-1 features; temperature is not used as a classification input, preserving independence for subsequent analysis of temperature-phenology relationships.

2.4 Phenology extraction

We determined the ice-on and ice-off dates from the classified ice state time series for each lake-year. To avoid detecting spurious mid-winter thaws or brief summer re-freezing events, we constrained transition detection to seasonal search windows: ice-off was sought between day-of-year 91 (April 1) and day-of-year 243 (August 31), while ice-on was sought beginning day-of-year 244 (September 1). These non-overlapping windows prevent logical inconsistencies in the detected phenology.

We defined ice-off as the first date when the lake transitioned from frozen to open water state and remained classified as water for at least two consecutive satellite observations. Similarly, we defined ice-on as the first date of the subsequent freeze-up when the lake transitioned to frozen state and remained classified as ice for at least two consecutive observations. With both ascending and descending Sentinel-1 orbits providing a median observation gap of 4 days at this latitude, this criterion typically requires sustained state persistence of approximately 8–16 days, filtering transient events while preserving sensitivity to true phenological transitions.

We then calculated the ice-free period as the number of days between ice-off and ice-on for each lake-year. We assigned null values to lakes lacking clear transitions due to data gaps, persistent cloud cover, or ambiguous classifications and excluded them from phenology statistics. We computed summary statistics including mean, median, standard deviation, and interquartile range across all valid lake-years, as well as stratified by geographic subregion and lake size class.

https://doi.org/10.5194/egusphere-2026-1135
Preprint. Discussion started: 17 March 2026

2.5 Phenology model comparison

To compare the SAR RF model with other methods for ice phenological timings, we used ERA5 daily average 2 m temperatures (Carver and Merose, 2023; Herbach et al. 2017; Hersbach et al., 2020) to calculate a continuous time series of both the accumulated degree day of thaw (ADDT) and accumulated degree day of freezing (ADDF) for ice thickness (Arp et al., 2015; Stefan, 1890). We calculated both of these metrics for each lake-year combination and used a seven-day switch window between freeze-thaw/thaw-freeze to ensure a sufficient duration for cumulative ice growth/melt before switching between ADDF and ADDT. We used $\alpha = 2$ as the Stefan equation coefficient to convert from degree-days to cm ice thickness. For inter-model comparison, we used the same ice-off and ice-on cutoff dates in the SAR model of August 31st and September 1st, respectively. We then computed the offsets between the SAR and ADD models by subtracting the ice-on and ice-off dates, where positive offsets indicate the SAR model predicting later than the ADD model and vice versa.

3 Results

3.1 Random-forest-derived ice phenology across the Arctic Coastal Plain

Ice phenology was successfully retrieved for 30,862 lakes (99.2% of the study population) for at least one year, with 95.5% having complete five-year records. Across all lakes and years, mean ice-off occurred on day-of-year (DOY) 163 (June 12; standard deviation = 14 days), ranging from DOY 91 to DOY 242. Mean ice-on occurred on DOY 278 (October 5; standard deviation = 15 days), ranging from DOY 244 to DOY 361. The resulting ice-free period averaged 115 days (standard deviation = 24 days), with individual lake-years spanning 6 to 268 days (Fig. S3). Interannual variability in ice timing was substantial (Figs. 2 and S5). The earliest regional mean ice-off occurred in 2021 (DOY 159), while the latest occurred in 2022 (DOY 170) (Fig. S5). Ice-free duration ranged from a mean of 107 days in 2022 to 123 days in 2019 (Fig. S5). Across all lake-years, ice-off and ice-on timing were moderately negatively correlated ($r = -0.43$), largely reflecting latitudinal gradients in both variables.

https://doi.org/10.5194/egusphere-2026-1135
Preprint. Discussion started: 17 March 2026

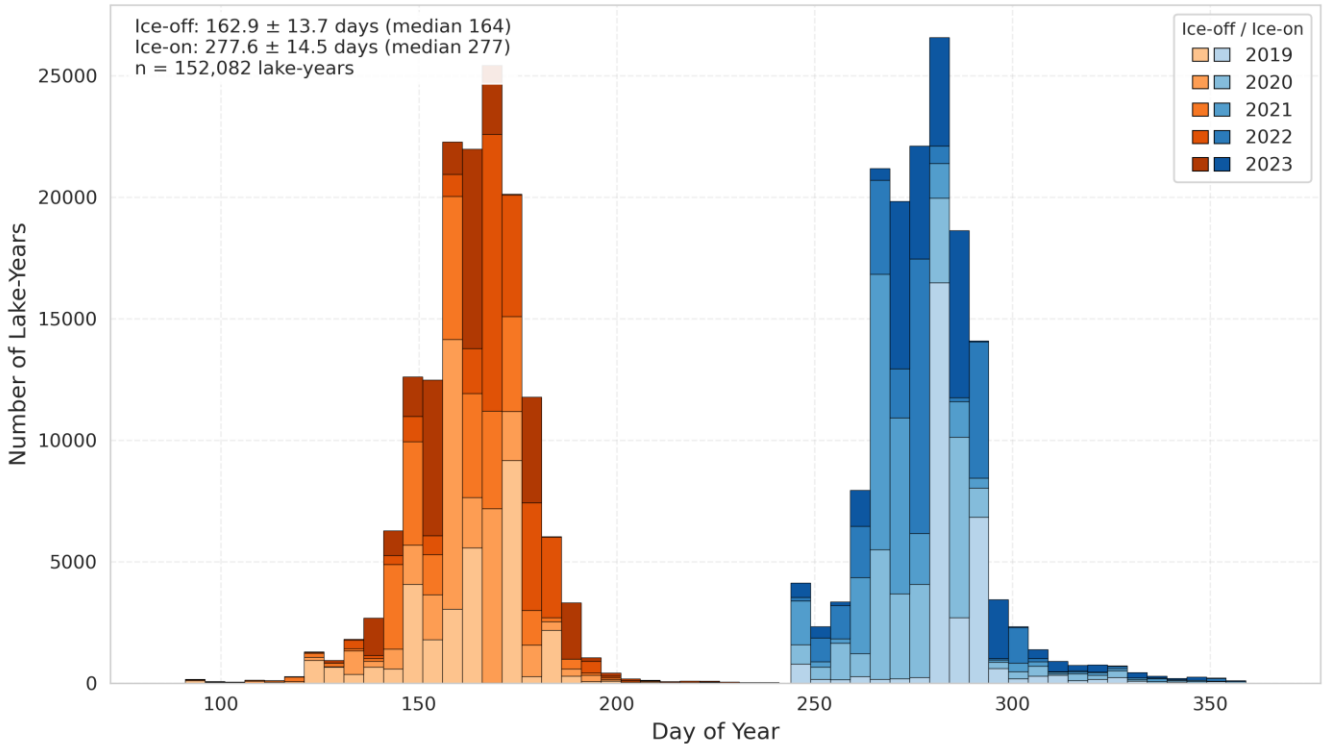

Figure 2: Distribution of ice phenology metrics across all lake-years (2019–2023), where increasing saturation corresponds to more-recent years. The red histogram indicates ice-off date, and the blue histogram indicates ice-on date.

Comparison of the ice phenology events derived from the RF model with the ADD metric shows relatively strong correspondence (Fig. 3). For ice-off dates, 59% of lakes align with ADD estimates within 2 revisits (roughly 12 days, but varying spatially and after loss of Sentinel-1 B), and for ice-on dates, 63% lakes align with ADD estimates within 2 revisits (Fig. 3). The median gap between the SAR detected ice-on or ice–off date and corresponding ADD metric was 7 days for thaws and 1 day for freezes. For ice-off dates, the RF model was earlier than the ADD estimate for 25% of the lake-years, later than the ADD estimate for 72% of the lake-years and selected the same date for 3% of the lake-years, suggesting a modest tendency toward delayed thaw detection relative to cumulative degree-day predictions (Fig. S15). For ice-on dates, the RF model was earlier than the ADD estimate for 51% of the lake-years, later than the ADD estimate for 42% of lake-years and selected the same date for 8% of lake-years, reflecting a more balanced distribution around the ADD metric during lake freeze-up (Fig. S15).

https://doi.org/10.5194/egusphere-2026-1135
Preprint. Discussion started: 17 March 2026

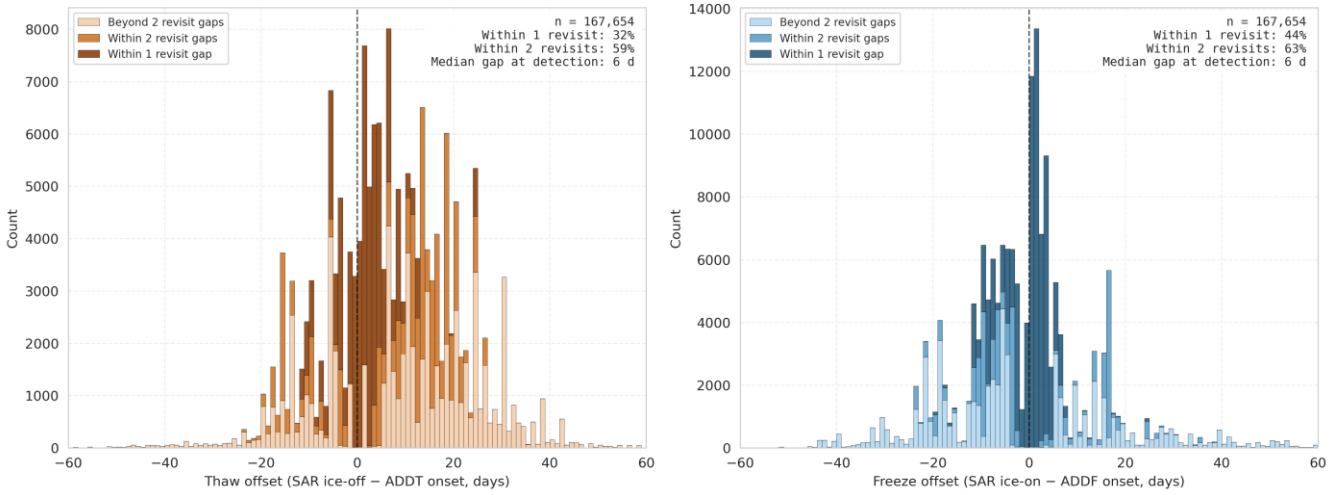

Figure 3: Histograms of the offset between ice phenology timings from SAR detection and the ADDT (a) and ADDF (b) algorithm. Negative values indicate SAR detects dates before ADDT/F, while positive values indicate SAR detects dates after the ADD metric. The histograms are shaded by SAR revisits (ie % within 1 revisit, within 2 revisits), where increasing saturation indicates data within shorter periods.

To evaluate the potential effects of latitudinal and morphologic controls on the offsets between the RF model and the ADD estimates for ice-on and thaw dates and ice-off and freeze dates, we implemented a series of statistical analyses including Kruskal-Wallis H-test, Mann-Whitney U-test, and Cliff's Delta (δ). For all lake-years, for ice-off dates, although statistically significant differences exist in lake morphometrics between cases where the RF model was earlier versus later than the ADD metric (H- and U-test $p << 0.05$), the effect sizes are very small ($\delta < 0.15$). This indicates that lake morphology does not play a significant role in explaining the observed offset between RF and ADD ice-off estimates. In contrast, latitude has a more significant effect size (H- and U-test $p << 0.05$; $\delta = -0.3683$), indicating that latitudinal effects likely explain some of the observed mismatch between RF and ADD ice-off timing. Lakes that the RF model identifies as ice-free earlier than the ADD estimate are generally found at lower latitudes while lakes where the RF model identifies the ice-free date later than the ADD estimate are generally located at higher latitudes. Similarly, for ice-on dates across all lake-years, morphology again exhibits statistically significant differences between groups, but with very weak effect sizes (H- and U-test $p << 0.05$; $\delta < 0.15$), while latitude has a stronger effect ($\delta = 0.343$).

Lakes identified by the RF model as ice-on earlier than the ADD estimate occur at higher latitudes, whereas those identified as ice-on later tend to lie farther south within the study region. Consistently, lakes classified as ice-on earlier by the RF model are substantially farther north than lakes classified as ice-off earlier ($\delta = -0.4109$), and lakes classified as ice-on later are located at higher latitudes than lakes classified as ice-off later ($\delta = 0.298$).

For lake-years where the offset between the RF model ice-on and ice-off dates and the ADD estimates is greater than 2 revisit gaps, the results are very similar. Within ice-off and ice-on dates, and comparisons between the two dates, morphometrics variables feature statistically significant differences between the groups but weak effect sizes (H- and U-test $p << 0.05$; $\delta <$

https://doi.org/10.5194/egusphere-2026-1135
Preprint. Discussion started: 17 March 2026

0.18) for differences between the RF model and ADD estimate dates. Latitude, however, continues to be an important variable for offsets between the RF model and ADD estimates. Within ice-off dates, the latitudinal statistical significance and large effect size between groups (H- and U-test $p << 0.05$; $\delta = -0.5019$) indicates that the RF model selects ice-off dates earlier than the ADD estimates at lower latitudes while selecting ice-off dates later than ADD estimates at higher latitudes. For ice-on dates, the RF model detects ice later than the ADD estimates ($\delta = 0.6256$) at lower latitudes and detects ice earlier than the ADD estimates at higher latitudes. Lakes where the RF detects ice-off earlier than the ADD estimates occur at lower latitudes ($\delta = -0.4867$) while lakes where the RF model detects ice-on earlier than the ADD occur at higher latitudes. Lakes where the RF detects ice-off later than the ADD estimates occur at higher latitudes ($\delta = 0.6474$) and lakes where the RF model detects ice-on later than the ADD estimates occur at lower latitudes.

3.2 Spatial patterns and latitudinal gradients in lake phenology

Ice phenology exhibited strong spatial structure across the study region (Fig. 4). Latitude was a dominant control on ice timing, with ice-free period decreasing by 32 days per degree northward ($r = -0.50$, $p < 0.001$; Fig. 4c, Fig. 5). This gradient reflects the combined effects of decreasing summer temperatures and shorter warm seasons with increasing latitude. Latitude correlations were strongest for ice-off timing ($r = 0.50$) and ice-free duration ($r = -0.50$), and weaker for ice-on timing ($r = -0.35$). Diagnostic tests indicated significant residual spatial autocorrelation (Moran's I = 0.45–0.47) reflecting unmeasured spatially-varying factors such as microclimate, permafrost properties, surface/subsurface hydrology, and topographic shading. Spatial Error Models were therefore fit using generalized moments estimation with K-nearest neighbour spatial weights (k=8). The spatial error parameter $\lambda \approx 0.68$ - 0.69 confirmed strong spatial autocorrelation from unmeasured regional factors, and filtered residuals showed negligible spatial autocorrelation (Moran's I ≈ -0.01 to -0.02), indicating adequate model specification.

https://doi.org/10.5194/egusphere-2026-1135
Preprint. Discussion started: 17 March 2026

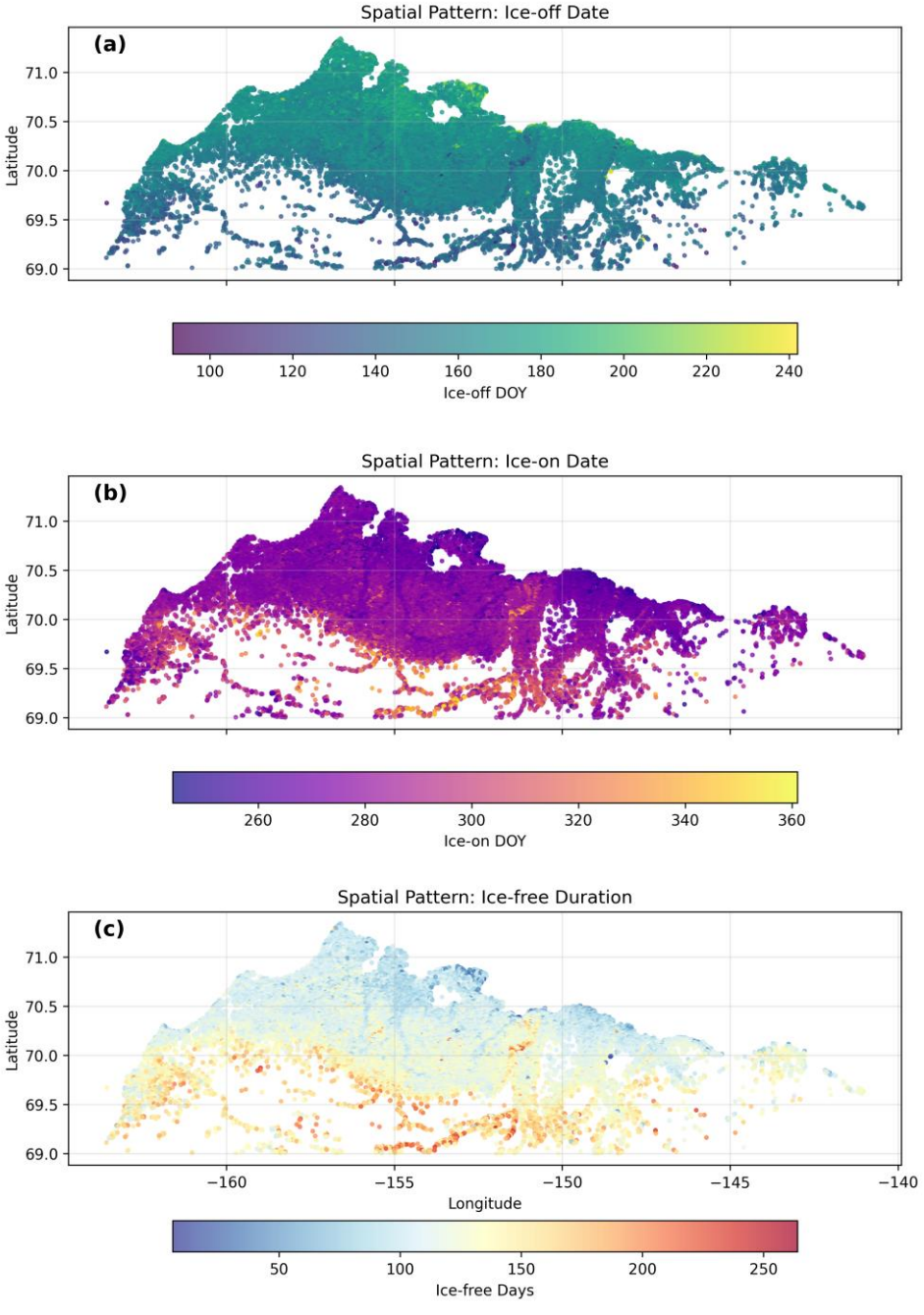

Figure 4: Spatial patterns in mean ice phenology (2019–2023): (a) ice-off date (day of year), (b) ice-on date, and (c) ice-free duration. Each point represents one lake.

https://doi.org/10.5194/egusphere-2026-1135
Preprint. Discussion started: 17 March 2026

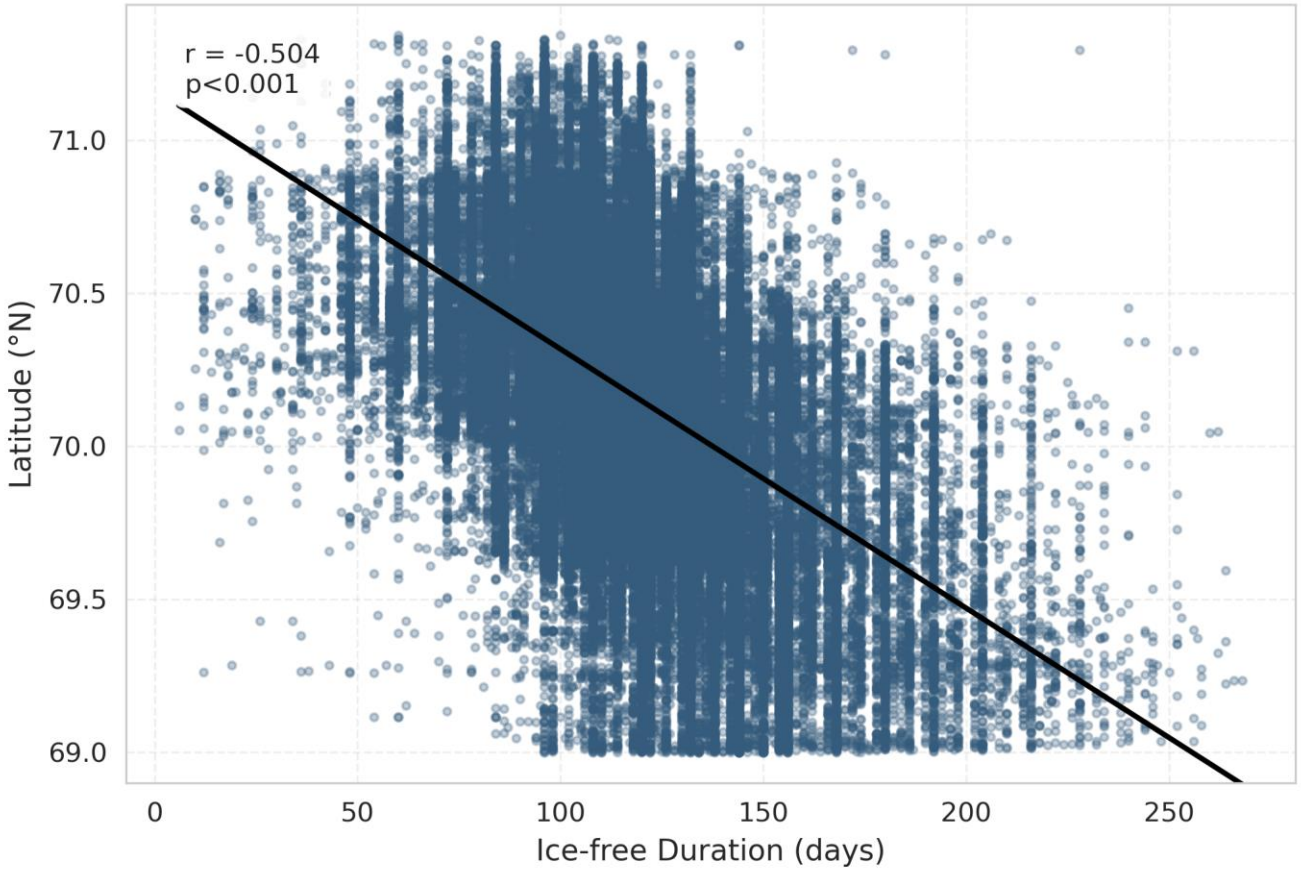

Figure 5: Relationship between latitude and ice-free duration. The black line shows the linear regression best-fit.

3.4 Morphometric relationships

Morphometric variables showed negligible correlations with mean spring temperature ($|r| \leq 0.11$ for SDI, circularity, convexity, and log-transformed area), confirming that morphometry is not confounded with spatial climate gradients. To assess the strength of morphometric controls on ice phenology, we modelled ice-off date, ice-on date, and ice-free duration as functions of mean spring temperature (April–June) and morphometric parameters using ordinary least squares regression. Lake area shows a statistically significant, but negligible correlation with ice-off and ice-on dates and ice-free duration (Fig. S6), indicating that although the relationship is detectable given the large sample size, it explains minimal variation in phenology. Lake circularity and SDI exhibit very weak but statistically significant correlations with ice-free duration, compared to the negligible association of ice-free duration and convexity that does not exhibit statistical significance (Fig. S7). Overall, morphometric correlation (area, circularity, SDI, and convexity) with ice phenology (ice-off date, ice-on date, and ice-free

https://doi.org/10.5194/egusphere-2026-1135
Preprint. Discussion started: 17 March 2026

duration) is weak (< ±0.14) (Fig. S8). Morphometry coefficients attenuated by approximately 20–25% under spatial correction but remained highly significant ($p<0.001$), confirming that morphometric effects on ice phenology are robust to spatial confounding. Multiple regression with temperature as a covariate showed that morphometric parameters explained an additional 1.4–1.9% of variance in ice phenology beyond temperature alone. OLS residuals showed significant spatial autocorrelation, so Spatial Error Models were used; all morphometric predictors remained significant after this correction, with shoreline development index (SDI) and convexity showing the largest effects.

Effect sizes were modest relative to temperature and interannual variability. Lakes with more complex shorelines (higher SDI) experienced shorter ice-free seasons (−3.3 days across the interquartile range), as did lakes with lower convexity (−3.1 days). Lake area and circularity showed smaller effects (+1.8 and +2.2 days, respectively) (Fig. 6). Increasing shoreline complexity and decreasing lake convexity shortens the ice-free period; while increasing lake area and circularity these lengthens the ice-free period.

Overall, morphometry plays a subordinate role to temperature in determining ice phenology at the regional scale, with temperature explaining 13-19% of variance compared to 1.4–1.9% for morphometric parameters. The relatively modest variance explained by temperature reflects the spatial autocorrelation structure in the data: much of the temperature signal is captured by latitude, which is implicitly included through the spatial error model. The spatial error parameter confirms that regional factors beyond point-level temperature such as coastal proximity, local topography, and regional weather patterns contribute substantially to ice timing variability.

https://doi.org/10.5194/egusphere-2026-1135
Preprint. Discussion started: 17 March 2026

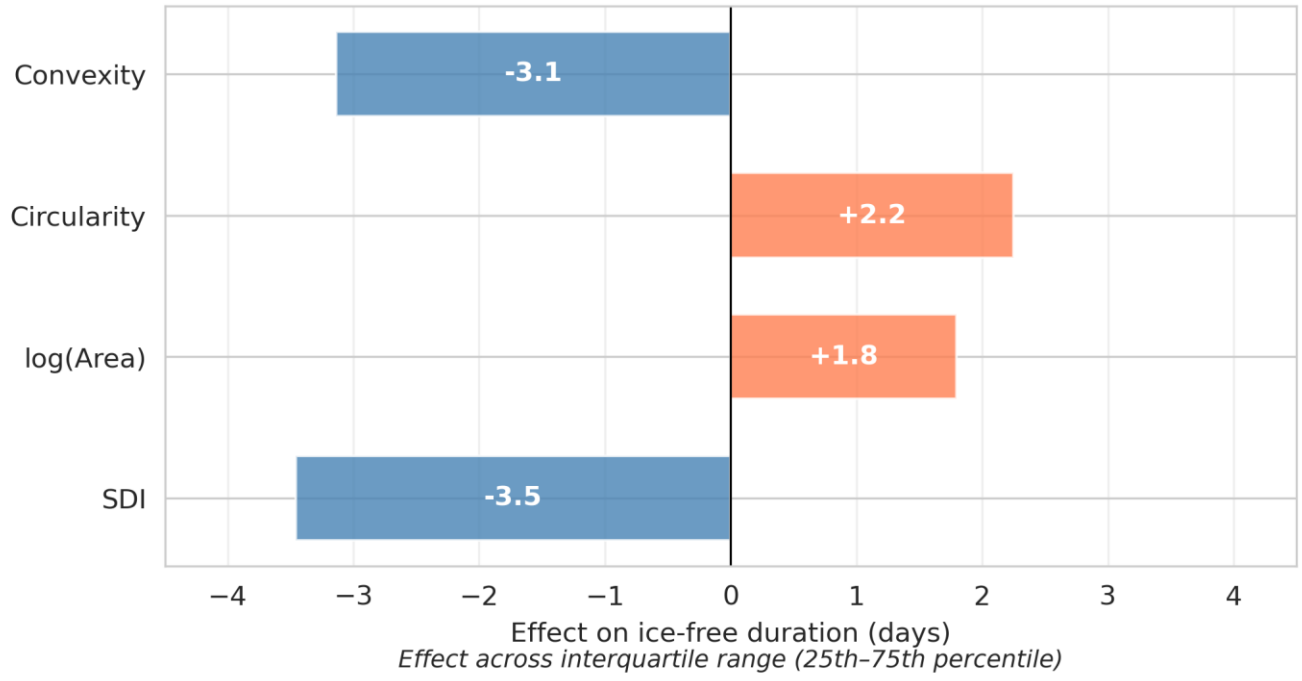

Figure 6: Spatially corrected effect of morphometric variables on ice-free duration, calculated across the interquartile range.

4 Discussion

4.1 Model Performance

While previous studies achieved high accuracy (95.8%) using sophisticated segmentation algorithms and extensive texture features on individual lakes (Hoekstra et al., 2020), such approaches are computationally prohibitive for analysis of tens of thousands of water bodies. Our simplified RF framework using six backscatter features achieves 91% accuracy while enabling consistent classification of ~30,000 lakes across multiple years, including during polar night and cloudy conditions when optical data are unavailable, demonstrating the feasibility of regional-scale ice phenology monitoring from satellite observations. Previous single-sensor SAR studies typically achieved accuracies on the order of ~80–85% (Surdu et al., 2014). The use of Sentinel-2 optical data to generate training labels for the RF classifier, combined with temperature-based quality control, enabled reliable classification even during the challenging transition seasons. The RF model feature importance (Fig. S2) further shows that using additional contextual information, such as land buffers surrounding the lakes, increased overall RF model accuracy compared to solely relying on lake pixels for ice-state determination (Tom et al., 2020).

The mean ice-free period of 115 days is consistent with limited in situ observations available for the region. Arp et al. (2015) reported ice-free periods of 80–110 days for instrumented lakes on the Arctic Coastal Plain during 2004–2013. Our results extend these findings across the full thermokarst lake population of roughly 30,000 lakes.

https://doi.org/10.5194/egusphere-2026-1135
Preprint. Discussion started: 17 March 2026

The bias in offsets we observe in the ice-off and ice-on dates between the RF model and the ADD estimates are likely due to inherent assumptions made in the RF and ADD models, as well as spatial scale differences in data resolutions (~10 m/pixel for Sentinel-1 vs ~30 km/pixel for ERA5). The RF and ADD models have fair agreeance, but they also exhibit inter-model biases that manifest differently during thaw and freeze. The accuracy of the RF model implicitly depends upon the assumed polarimetric scattering model, wherein changes in radar backscatter within and between polarization channels are assumed to be driven by the systematic difference in polarized backscatter between ice and liquid water (Jeffries et al. 1994; Beaven 1995). In reality, dielectric permittivity changes due to partial surface melting, the presence of snow, changes in snow water equivalent, and ice metamorphism can all introduce changes to SAR backscatter that can complicate the interpretation of a simple water phase transition (Paul et al., 2017; Marin et al., 2020; Lund et al., 2022; Veijola et al., 2024). These confounding effects can be particularly apparent during the shoulder seasons making satellite observation of ice phenology y difficult (Posch et al., 2024). Additionally, it is possible that the Sentinel-1 descending track (~61% of scenes) images, which are acquired between 7:00-9:00 AM AKST may also introduce variability in predicted ice phenology with the RF model due to diurnal freeze/thaw processes during the shoulder seasons (Fig. S13). Likewise, the use of ADD to model thermal diffusion through the ice cover implicitly assumes a purely 1-dimensional diffusive heat transfer at the air-water surface interface, neglecting lateral heat transfer or wind-driven thermal advection. We further do not consider the effect of snowpack cover, which serves to delay ice-off timing, due to the lack of sufficiently accurate, high spatial resolution snow depth and snow water equivalent products. This deliberate choice of model simplicity could explain some of the observed offset between RF and ADD model ice-on and ice-off calls, particularly during ice thaw when the presence of snowpack can considerably impact the timing of ice-off (Pouw et al., 2023). This epistemic uncertainty propagates into both models' ability to predict exact dates for ice phenology. The difficulty in determining thaw onset is exemplified when comparing the bias in offsets between the RF and ADD models in figure 6, where the offset of thaw has 32% and 59% of the lakes within one and two revisits, respectively, whereas the offset for freeze has 44% and 63% of lakes within one and two revisits. The tighter distribution and smaller skew of the freeze offsets is consistent with a relative improvement in predicting ice-on/freeze up compared to ice-off/thaw onset (Fig. 6). While freeze-up is still a complex process, it is more strongly controlled by a unidirectional temperature change, resulting in a more gradual process that can be more effectively predicted based on temperature trends, which results in the observed tighter distribution of offsets. Despite the simple radar scattering and thermodynamic models employed here, each model exhibits decent predictive power for ice phenology and timing, and the inter-model biases are physically consistent.

4.2 Latitudinal and morphometric effects on ice phenology

The primary control on thermokarst lake ice phenology on the Alaska North Slope is latitude, which implicitly includes temperature. Latitude also incorporates other factors such as coastal proximity, topography, and local weather patterns. As a result, these likely also contribute to ice timing variability in addition to temperature. The strong latitudinal gradient in ice-free duration (30 days per degree northward; Fig. 5) is steeper than the ~6 days per degree reported for seven deep lakes across a broader latitudinal range (49–61°N) in the Canadian cordillera (Carmack et al., 2014), consistent with the heightened climate

https://doi.org/10.5194/egusphere-2026-1135
Preprint. Discussion started: 17 March 2026

sensitivity of lakes near the northern limits of the seasonal ice zone. This sensitivity implies that continued Arctic warming could produce disproportionately large changes in ice phenology for these northernmost lakes, with consequently disproportionate effects on future green-house gas emissions (Walter Anthony et al., 2018).

Our statistical analysis suggests that the offset between the RF and ADD model ice-on and ice-off dates is due in part to latitudinal effects. This is particularly so for lakes for which the RF-ADD model offset is greater than 2 revisit gaps (> 12 days). Lakes at lower latitudes are more likely to have ice-off detected by the RF model earlier than the ADD estimates and ice-on detected later relative to the ADD estimates. Lakes at higher latitudes have ice-off detected by the RF model later than the ADD estimates and ice-on earlier relative to the ADD estimates. This indicates that the RF model detects a longer ice-free period for lower latitude lakes and a shorter ice-free period for higher latitudes relative to the ADD estimates, suggesting that the ADD model is more conservative in predicting ice-free duration at lower latitudes whereas at higher latitudes, the RF model is more conservative.

The latitudinal gradient in offsets between the models may be explained through ice thickness variation as a function of latitude, the RF model not accounting for ice thickness, topography and microclimate, and differences in the spatial resolution of data. Given that lower latitudes have higher temperatures and are located further inland, they may have thinner ice overall and more complex freezing and thawing dynamics than lakes at higher latitudes. Meanwhile, these higher latitude lakes experience cooler temperatures and are more exposed to the Arctic Ocean thus freezing more rapidly. Furthermore, it is likely that the topographic gradient from the Brooks Range in the south to the low-elevation ACP in the north of our study area has an effect on the thermal budgeting of the lakes, owing to high-relief, radiation shadowing, and aspect differences that affect SAR backscatter through the imaging geometry (e.g. layover and shadowing). Additionally, the higher resolution of the SAR observations (~10 m/pixel) compared to the ERA5 temperature data (~30 km/pixel) may cause the RF model to capture thawing and freezing more precisely than the lower resolution ADD estimates of ice thickness by accounting for other thermal effects around lakes and the local microclimate and topography that are beyond the resolution capabilities of the ERA5 data.

The morphometric relationships we identified provide insight into the physical controls on ice phenology beyond geographic location. Morphology regulates heat transfer from a lake's surroundings to the lake itself (Basu et al., 2024; Brown and Dugay, 2010) ultimately modulating the coupled effects of air temperature and latitude for an individual lake.

Shoreline development index (SDI) and convexity showed the largest effects after spatial correction (~3 days across typical ranges), while lake area and circularity showed smaller but significant effects (~1–2 days) (Fig. 6). Higher SDI, indicating a more complex shoreline, generally suggests shorter ice-free periods, with the onset of freezing occurring earlier in the year and onset of thaw beginning later. Similarly, lower convexity, associated with higher boundary concavity or irregularity (Bozeman and Pilling, 2013), shortens the ice-free period due to ice-on occurring at an earlier date. Conversely, higher circularity lakes tend to remain ice-free longer because they freeze later and thaw earlier in the year.

These patterns may reflect thermal sheltering in inlets and reduced fetch, which promotes ice growth earlier in the year (Basu et al., 2024). Smaller fetch results in reduced wind speeds, which facilitates the growth of ice crystals, while higher wind speeds can break up the initially forming ice layer. (Brown and Dugay, 2010). Ice growth typically begins along sheltered parts

https://doi.org/10.5194/egusphere-2026-1135
Preprint. Discussion started: 17 March 2026

of the lakes and along the shore (Ashton, 1986), due in part to the wind-effect but also because of the shallower depths, which are more sensitive to temperature changes (Kirillin, et al., 2012). Irregular lakes have more shoreline per area, helping to initiate ice growth earlier than more circular or compact lakes. Lower convexity may also be related to overall shallower depths (Zhan et al., 2023), suggesting that deeper lakes have longer ice-free periods than shallower lakes. This likely corresponds to the patterns we identify with lake area, where ice free period increases with lake area. Lake depths tend to scale with area (Cael and Seekell, 2022); thus, these larger and deeper lakes remain ice-free longer because they begin freezing later in the year likely due to their greater thermal inertia. Indeed, lake depth has been found to be a significant control on the timing of ice-off conditions for thermokarst lakes in this region (Arp et al., 2015).

Overall, morphometry explained only 1.5–2% of variance beyond temperature, indicating that climate remains the dominant control on regional ice phenology. Nonetheless, morphology plays a significant role in regulating the climatic impact for thermokarst lakes on the Alaska North Slope.

4.3 Implications for GHG emissions and Arctic change

Based on our results, Arctic thermokarst lakes are likely to experience pronounced effects on ice phenology due to global climate change. The strong latitudinal-temperature dependence suggests that increased warming will likely increase the ice free-period, which will further contribute to greenhouse gas emissions (Guo et al. 2020; Zhuang et al., 2023). Because larger lakes have longer ice-free durations, their potential contribution to GHG emissions may increase. However, these effects may be dwarfed by the sheer number of smaller lakes, which likely have a higher potential contribution. Furthermore, if larger lakes are indeed deeper, than they may also be less efficient emitters of methane due to increased oxidation that occurs in deeper water columns. Recent work (Levenson et al., 2025) found that thermokarst lakes in previously unglaciated landscapes underlain with continuous permafrost, including our study area, are projected to decrease in overall total area under projected climate scenarios. This reduction in total area may have direct effects on average lake depth and consequently emission potential, as shallower lakes and ponds exhibit higher methane emissions than deeper lakes (Manasypov et al., 2023).

The phenology baseline established here provides a foundation for detecting future changes in thermokarst lake ice regimes that can be incorporated with other Arctic remote sensing studies of methane emissions from thermokarst lakes (Elder et al., 2020; Engram and Walter Anthony, 2024; Kyzivat and Smith, 2023). Future monitoring efforts can be leveraged in conjunction with these results to assess whether ice-free periods increase as predicted by climate models. Lastly, upcoming higher-resolution spaceborne methane measurements (e.g., MethaneSAT, Carbon Mapper, GHGSat (McLinden et al., 2024)) could be leveraged in conjunction with this ice phenology and timing observational method to directly observe the ice-phenology-emission relationship from the individual lake-scale to the regional-scale and determine the relative importance of numerous small lakes vs. fewer larger lakes in consideration of GHG emission budgeting.

https://doi.org/10.5194/egusphere-2026-1135
Preprint. Discussion started: 17 March 2026

5 Conclusion

This study presents the first comprehensive analysis of ice phenology across the Alaska North Slope thermokarst lake population. Using a RF classifier trained on Sentinel-2 optical labels and applied to Sentinel-1 SAR imagery, we achieved 91% accuracy for ice state classification and retrieved phenology for 30,862 lakes over five years (2019–2023).

The mean ice-free period is 115 days, with ice-off occurring in mid-June (DOY 163) and ice-on in early October (DOY 278). Latitude exerts dominant control on ice timing, with ice-free duration decreasing by 30 days per degree northward. Morphometric predictors showed modest but significant effects after spatial correction, with shoreline development index and convexity each contributing ~3 days variation across typical lake ranges.

These results provide essential baseline data for monitoring how thermokarst lake dynamics respond to continued Arctic warming, with implications for regional carbon cycling and climate feedbacks. The lake-specific ice phenology dates also provide critical timing constraints for methane emission models and for planning targeted high-resolution observation campaigns.

Code and data availability

Sentinel-1 and Sentinel-2 imagery were accessed through Google Earth Engine (https://earthengine.google.com). ERA5 reanalysis data are available from the Copernicus Climate Data Store (https://cds.climate.copernicus.eu). TROPOMI methane data were obtained from the Copernicus Atmosphere Data Store. The Alaska Lake and Pond Occurrence Dataset (ALPOD) is available from the ORNL DAAC (doi:10.3334/ORNLDAAC/2399). Processed ice phenology data and analysis code are archived at https://github.com/bradleylab/thermokarst-lakes-alaska.

Interactive computing environment

All code used in this study is provided in the form of Jupyter Notebooks within the provided Zenodo and GitHub repositories. Each notebook lists the necessary Python packages and calls to Google Cloud storage buckets through Washington University in St. Louis. These Jupyter Notebooks can be directly downloaded to run locally or in the cloud, and the GitHub repository can be forked and cloned for execution and reproduction.

Author contributions

Conceptualization: all authors. Data curation: A.L.N., A.S.B., R.J.M. Formal analysis: all authors. Investigation: C.G.L., A.L.N., A.S.B., R.J.M. Methodology: all authors. Software: C.G.L., A.S.B. Writing: all authors. Supervision: R.J.M., C.C.M. A.L.N. and C.G.L contributed equally to the manuscript.

https://doi.org/10.5194/egusphere-2026-1135
Preprint. Discussion started: 17 March 2026

Competing interests

The authors declare that they have no conflict of interest.

Acknowledgements

We thank the Google Earth Engine team for providing computational resources and for open access to satellite data (Gorelick et al., 2017). Hersbach et al, (2017) was downloaded from the Copernicus Climate Change Service (C3S) Climate Data Store. We thank C3S for allowing us to redistribute the data. The results contain modified Copernicus Climate Change Service information 2022. Neither the European Commission nor ECMWF is responsible for any use that may be made of the Copernicus information or data it contains. We thank the Natural Earth for vector data provided through Amazon Web Services used in figure map generation.

We would additionally like to thank Isabel Lopez for assistance in initial project conceptualization and planning and preliminary manual data analysis. Furthermore, we thank Alisa Oates and Amelia Mogul for assistance in preliminary work manually validating an earlier version of the RF model used in this study.

We used generative AI (gpt-5.2, opus-4.6, and gemini-3) to assist with computational code associated with this study. Initial code was produced and refined through iterative prompting and subsequently reviewed and manually revised by the authors.

Financial support

This research was supported by the Washington University Department of Earth, Environmental, and Planetary Sciences and by a National Science Foundation Graduate Research Fellowship and the Ann W. and Spencer T. Olin-Chancellor's fellowship to A.N.

This material is based upon work supported by the National Science Foundation's Graduate Research Fellowship Program (under Grant No. DGE 2139839). Any opinions, findings, and conclusions or recommendations expressed in this material are those of the author(s) and do not necessarily reflect the views of the National Science Foundation.

References

Arp, C. D., Jones, B. M., Urban, F. E., and Grosse, G.: Hydrogeomorphic processes of thermokarst lakes with grounded-ice and floating-ice regimes on the Arctic coastal plain, Alaska, Hydrol. Process., 25, 2422–2438, 2011.

Arp, C. D., Jones, B. M., Liljedahl, A. K., Hinkel, K. M., and Welker, J. A.: Depth, ice thickness, and ice-out timing cause divergent hydrologic responses among Arctic lakes, Water Resour. Res., 51, 9379–9401, 2015.

Ashton, G.D.: River and Lake Ice Engineering. Water Resources Publications, Littleton, CO, 1986.

https://doi.org/10.5194/egusphere-2026-1135
Preprint. Discussion started: 17 March 2026

Bartsch, A., Pointner, G., Leibman, M. O., Dvornikov, Y. A., Khomutov, A. V., and Trofaier, A. M.: Circumpolar mapping of ground-fast lake ice, Front. Earth Sci., 5, 12, 2017.

Bartsch, A., Strozzi, T., and Nitze, I.: Permafrost Monitoring from Space, Surveys in Geophysics, 2023.

Basu, A., Culpepper, J., Blagrave, K., & Sharma, S.: Phenological shifts in lake ice cover across the Northern Hemisphere: A glimpse into the past, present, and the future of lake ice phenology. Water Resour. Res., 60, 2024.

Beaven, S. G.: Sea Ice Radar Backscatter Modeling, Measurements, and the Fusion of Active and Passive Microwave Data. Radar Remote Sensing Laboratory, The University of Kansas Center for Research, Inc., 1995.

Bozeman, J. R., & Pilling, M.: The Convexity Ratio and Applications, Scientiae Mathematicae Japonicae, 76(1), 47-53, 2013.

Breiman, L.: Random Forests, Machine Learning, 45, 5-32, 2001.

Brown, L. C., & Duguay, C. R.: The response and role of ice cover in lake-climate interactions. Progress in Physical Geography: Earth and Environment, 34(5), 671-704, 2010.

Cael, B.B. and Seekell, D.: A theory for the relationship between lake surface area and maximum depth. Limnol. Oceanogr. Lett, 7, 527-533, 2022.

Carmack, E. C., Vagle, S., Morrison, J., and Laval, B. E.: Space-for-time proxy for climate change in deep lakes in the Canadian cordillera: Seasonality along a latitudinal climate gradient, J. Great Lakes Res., 40, 608–617, 2014.

Carver, R. W., and Merose, A.: ARCO-ERA5: An Analysis-Ready Cloud-Optimized Reanalysis Dataset. 22nd Conference on AI for Environmental Science. American Meterological Society, 4A.1, 2023.

Duguay, C.R., Flato, G.M., Jeffries, M.O., Ménard, P., Morris, K. and Rouse, W.R. (2003), Ice-cover variability on shallow lakes at high latitudes: model simulations and observations. Hydrol. Process., 17, 3465-3483, 2003.

Elder, C. D., Thompson, D. R., Thrope, A. K., Hanke, P., Walter Anthony, K. M., Miller, C. E.: Airborne Mapping Reveals Emergent Power Law of Arctic Methane Emissions, Geophysical Research Letters, 47, 3, 2020.

Engram, M., and Walter Anthony, K.: Synthetic aperture radar (SAR) detects large gas seeps in Alaska lakes. Environmental Research Letters, 19, 2024.

Gorelick, N., Hancher, M., Dixon, M., Ilyushchenko, S., Thau, D., and Moore, D.: Google Earth Engine: Planetary-scale geospatial analysis for everyone. Remote Sensing of Environment, 2017.

Guo M., Zhuang, W., Tan, Z., Shurpali, N., Juutinen, S., Kortelainen, P., and Martikainen, P. J.: Rising methane emissions from boreal lakes due to increasing ice-free days, Environmental Research Letters, 15, 6, 2020.

Hall, D. K., Fagre, D. B., Klasner, F., Linebaugh, G., and Liston, G. E.: Analysis of ERS 1 synthetic aperture radar data of frozen lakes in northern Montana and implications for climate studies. Journal of Geophysica Research Oceans, 99, C11, 22473-22482, 1994.

Hall, D., Riggs, G.A., and Salomonson, V. V.: Development of methods for mapping global snow cover using moderate resolution imaging spectroradiometer data, Remote Sensing of Environment, 54, 2, 127-40, 1995.

Hersbach, H., Bell, B., Berrisford, P., Hirahara, S., Horányi, A., Muñoz-Sabater, J., Nicolas, J., Peubey, C., Radu, R., Schepers, D., Simmons, A., Soci, C., Abdalla, S., Abellan, X., Balsamo, G., Bechtold, P., Biavati, G., Bidlot, J., Bonavita, M., De Chiara, G., Dahlgren, P., Dee, D., Diamantakis, M., Dragani, R., Flemming, J., Forbes, R., Fuentes, M., Geer, A., Haimberger, L.,

https://doi.org/10.5194/egusphere-2026-1135
Preprint. Discussion started: 17 March 2026

Healy, S., Hogan, R.J., Hólm, E., Janisková, M., Keeley, S., Laloyaux, P., Lopez, P., Lupu, C., Radnoti, G., de Rosnay, P., Rozum, I., Vamborg, F.,Villaume, S., Thépaut, J-N.: Complete ERA5: Fifth generation of ECMWF atmospheric reanalyses of the global climate. Copernicus Climate Change Service (C3S) Data Store (CDS), 2017.

Hersbach, H., Bell, B., Berrisford, P., Hirahara, S., Horányi, A., Muñoz-Sabater, J., Nicolas, J., Peubey, C., Radu, R., Schepers, D., Simmons, A., Soci, C., Abdalla, S., Abellan, X., Balsamo, G., Bechtold, P., Biavati, G., Bidlot, J., Bonavita, M., De Chiara, G., Dahlgren, P., Dee, D., Diamantakis, M., Dragani, R., Flemming, J., Forbes, R., Fuentes, M., Geer, A., Haimberger, L., Healy, S., Hogan, R. J., Hólm, E., Janisková, M., Keeley, S., Laloyaux, P., Lopez, P., Lupu, C., Radnoti, G., de Rosnay, P., Rozum, I., Vamborg, F., Villaume, S., and Jean-Noël Thépaut: The ERA5 global reanalysis, Q. J. R. Meteorol. Soc., 146, 1999–2049, 2020.

Heslop, J. K., Walter Anthony, K. M., Winkel, M., Sepulveda-Jauregui, A., Martinez-Cruz, K., Bondurant, A., Gross, G., and Liebner, S.: A synthesis of methane dynamics in thermokarst lake environments, Earth-Science Reviews, 2020.

Higgins, S. N., Desjardins, C. M., Drouin, H., Hrenchuk, L. E., & van der Sanden, J. J.: The role of climate and lake size in regulating the ice phenology of boreal lakes. Journal of Geophysical Research: Biogeosciences, 126, 2021.

Hinkel, K. M., Sheng, Y., Lenters, J. D., Lyons, E. A., Beck, R. A., Eisner, W. R., and Wang, J.: Thermokarst Lakes on the Arctic Coastal Plain of Alaska: Geomorphic Controls on Bathymetry, Permafrost and Periglacial Processes, 23, 3, 218-230, 2012.

Hoekstra, M., Jiang, M., Clausi, D. A., and Duguay, C.: Lake ice-water classification of RADARSAT-2 images by integrating IRGS segmentation with pixel-based random forest labeling, Remote Sens. (Basel), 12, 1425, 2020.

Hutchinson, G. E.: A Treatise on Limnology, Vol. 1: Geography, Physics, and Chemistry, John Wiley & Sons, New York, NY, 1957.

In 'T Zandt, M. H., Liebner, S., and Welte, C. U.: Roles of Thermokarst Lakes in a Warming World, Trends in Microbiology, 28, 9, 2020.

Jeffries, M. O., Morris, K., Weeks, W. F., and Wakabayashi, H.: Structural and stratigraphie features and ERS 1 synthetic aperture radar backscatter characteristics of ice growing on shallow lakes in NW Alaska, winter 1991-1992, Journal of Geophysical Research Oceans, 99, C11, 22459-22471, 1994.

Kirillin, G., Leppäranta, M., Terzhevik, A. et al.: Physics of seasonally ice-covered lakes: a review. Aquat Sci 74, 659–682, 2012.

Latifovic, R., and Pouliot, D.: Analysis of climate change impacts on lake ice phenology in Canada using the historical satellite data record, Remote Sensing of Environment, 106, 4, 2007.

Lafrenière, M. J., and Lamoureux, S. F.: Effects of changing permafrost conditions on hydrological processes and fluvial fluxes, Earth-Science Reviews, 191, 212-223, 2019.

Levenson, E., Cooley, S. W., and Mullen, A.: ABoVE: Alaska Lake and Pond Occurrence, https://doi.org/10.3334/ORNLDAAC/2399, 2025.

Lund, J., Forster, R. R., Deeb, E. J., Liston, G. E., Skiles, S. M., and Marshall, H.: Interpreting Sentinel-1 SAR Backscatter Signals of Snowpack Surface Melt/Freeze, Warming, and Ripening, through Field Measurements and Physically-Based SnowModel, Remote Snsing, 14 (16), 4002, 2022.

Manasypov, R., Fan, L., Lim, A. G., Krickov, I. V., Pokrovsky, O. S., Kuzyakov, Y., and Dorodnikov, M.: Size matters: Aerobic methane oxidation in sediments of shallow thermokarst lakes, Global Change Biology, 2023.

https://doi.org/10.5194/egusphere-2026-1135
Preprint. Discussion started: 17 March 2026

Matthews, E., Johnson, M. S., Genovese, V., Du, J., and Bastviken, D.: Methane emission from high latitude lakes: Methane-centric lake classification and satellite-driven annual cycle of emissions. Scientific Reports, 10, 1, 2020.

Marin, C., Bertoldi, G., Premier, V., Callegari, M., Brida, C., Hürkamp, K., Tschiersch, J., Zebisch, M., and Notarnicola, C., Use of Sentinel-1 radar observations to evaluate snowmelt dynamics in alpine regions, The Cryosphere, 14, 935-956, 2020.

McLinden, C. A., Griffin, D., Davis, Z., Hempel, C., Smith, J., Sioris, C., Nassar, R., Moeini, O., Legault-Ouellet, E., and Malo, A.: An Independent Evaluation of GHGSat Methane Emissions: Performance Assessment

Mu, C., Lei, P., Mu, M., Zhang, C., Zhou, Z., Song, J., Jia, Y., Fan, C., Peng, X., Zhang, G., Yang, Y., Wang, L., Li, D., Song, C., Wang, G., and Zhang, Z.: Methane emissions from thermokarst lakes must emphasize the ice-melting impact on the Tibetan Plateau, Nature Communications, 16, 1, 2025.

Mullen, A. L., Watts, J. D., Rogers, B. M., Carroll, M. L., Elder, C. D., Noomah, J., Williams, Z., Caraballo-Vega, J. A., Bredder, A., Rickenbaugh, E., Levenson, E., Cooley, S. W., Hung, J. K. Y., Fiske, G., Potter, S., Yang, Y., Miller, C. E., Natali, S. M., Douglas, T. A., and Kyzivat, E. D.: Using high-resolution satellite imagery and deep learning to track dynamic seasonality in small water bodies, Geophysical Research Letters, 50, 7, 2023.
Mullissa, A.; Vollrath, A.; Odongo-Braun, C.; Slagter, B.; Balling, J.; Gou, Y.; Gorelick, N.; Reiche, J. Sentinel-1 SAR Backscatter Analysis Ready Data Preparation in Google Earth Engine. Remote Sensing, 13, 10, 2021.

Muster, S., Roth, K., Langer, M., Lange, S., Cresto Aleina, F., Bartsch, A., Morgenstern, A., Grosse, G., Jones, B., Sannel, A. B. K., Sjöberg, Y., Günther, F., Andresen, C., Veremeeva, A., Lindgren, P. R., Bouchard, F., Lara, M. J., Fortier, D., Charbonneau, S., Virtanen, T. A., Hugelius, G., Palmtag, J., Siewert, M. B., Riley, W. J., Koven, C. D., and Boike, J.: PeRL: a circum-Arctic Permafrost Region Pond and Lake database, Earth Syst. Sci. Data, 9, 317–348, 2017.

Pedregosa, F., Varoquaux, G., Gramfort, A., Michel, V., Thirion, B., Grisel, O., Blondel, M., Prettenhofer, P., Weiss, R., Dubourg, V., Vanderplas, J., Passos, A., Cournapeau, D., Brucher, M., Perrot, M., and Duchesnay, E.: Scikit-learn: Machine learning in Python, J. Mach. Learn. Res., 12, 2825–2830, 2011.

Posch, C., Abermann, J., and Silva, T.: Lake ice break-up in Greenland: timing and spatiotemporal variability, The Cryosphere, 18, 2035-2059, 2024.

Pouw, A. F., Pour, H. K., and MacLean, A.: Mapping snow depth on Canadian sub-arctic lakes using ground-penetrating radar, The Cryosphere, 17, 2367-2385, 2023.

Rantanen, M., Karpechko, A. Y., Lipponen, A., Nordling, K., Hyvärinen, O., Ruosteenoja, K., Vihma, T., and Laaksonen, A.: The Arctic has warmed nearly four times faster than the globe since 1979, Commun. Earth Environ., 3, 168, 2022.

Riggs, G. A., Hall, D. K., and Román, M. O.: Overview of NASA's MODIS and VIIRS snow-cover Earth System Data Records, Earth Syst. Sci. Data, 8, 215–226, 2016.

Schuur, E. A. G., McGuire, A. D., Schädel, C., Grosse, G., Harden, J. W., Hayes, D. J., Hugelius, G., Koven, C. D., Kuhry, P., Lawrence, D. M., Natali, S. M., Olefeldt, D., Romanovsky, V. E., Schaefer, K., Turetsky, M. R., Treat, C. C., and Vonk, J. E.: Climate change and the permafrost carbon feedback, Nature, 520, 7546, 2015.

Seekell, D., Cael, B. B., Byström, P.: Problems With the Shoreline Development Index—A Widely Used Metric of Lake Shape, Geophysical Research Letters, 49, 10, 2022.

Sentinel-Hub: Sentinel-2 cloud detector, https://github.com/sentinel-hub/sentinel2-cloud-detector, 2025.

Serreze, M. C., and Barry, R. G.: Processes and impacts of Arctic Amplification: A research synthesis, Global and Planetary Change, 77, 1-2, 2011.

https://doi.org/10.5194/egusphere-2026-1135
Preprint. Discussion started: 17 March 2026

Skakun, S., Wevers, J., Brockmann, C., Doxani, G., Aleksandrov, M., Batič, M., Frantz, D., Gascon, F., Gómez-Chova, L., Hagolle, O., López-Puigdollers, D., Louis, J., Lubej, M., Mateo-García, G., Osman, J., Peressutti, D., Pflug, B., Puc, J., Richter, R., Roger, J.-C., Scaramuzza, P., Vermote, E., Vesel, N., Zupanc, A., and Žust, L.: Cloud Mask Intercomparison eXercise (CMIX): An evaluation of cloud masking algorithms for 8 and Sentinel-2, Remote Sens. Environ., 274, 112990, 2022.

Smits, A. P., Gomez, N. W., Dozier, J., & Sadro, S.: Winter climate and lake morphology control ice phenology and under-ice temperature and oxygen regimes in mountain lakes. Journal of Geophysical Research: Biogeosciences, 126, 2021.

Stefan, J.: On the theory of ice formation, with particular regard to ice formation in the polar sea, Sitz. Ber. Kais. Akad. Wiss. Wien, 98, 965-983, 1890.

Streletskiy, D. A., Maslakov, A., Grosse, G., Shiklomanov, N. I., Farquharson, L., Zwieback, S., Iwahana, G., Bartsch, A., Liu, L., Strozzi, T., Lee, H., and Debolskiy, M. V.: Thawing permafrost is subsiding in the Northern Hemisphere-Reivew and perspectives, Environmental Research Letters, 20, 1, 2025.

Surdu, C. M., Duguay, C. R., Brown, L. C., and Fernández Prieto, D.: Response of ice cover on shallow lakes of the North Slope of Alaska to contemporary climate conditions (1950--2011): Radar remote-sensing and numerical modeling data analysis, Cryosphere, 8, 167–180, 2014.

Surdu, C. M., Duguay, C. R., and Fernández Prieto, D.: Evidence of recent changes in the ice regime of lakes in the Canadian High Arctic from spaceborne satellite observations, Cryosphere, 10, 941–960, 2016.

Tom, M., Aguilar, R., Imhof, P., Leinss, S., Baltsavias, E., and Schindler, K.: Lake ice detection from Sentinel-1 Sar with deep learning, ISPRS Ann. Photogramm. Remote Sens. Spat. Inf. Sci., V-3–2020, 409–416, 2020.

Veijola, K., Cohen, J., Mäkynen, M., Lemmetyinen, J., Praks, J., and Cheng, B.: X- and Ku-Band SAR Backscattering Signatures of Snow-Covered Lake Ice and Sea Ice, Remote Sensing, 16 (2), 369, 2024.

Walter Anthony, K., Schneider von Deimling, T., Nitze, I., Frolking, S., Emond, A., Daanen, R., Anthony, P., Lindgren, P., Jones, B., and Grosse, G.: 21st-century modeled permafrost carbon emissions accelerated by abrupt thaw beneath lakes, Nat. Commun., 9, 3262, 2018.

West, W. E., Creamer, K. P., and Jones, S. E.: Productivity and depth regulate lake contributions to atmospheric methane, Limnology and Oceanography, 61, S1, 2016.

Wik, M., Varner, R. K., Anthony, K. W., MacIntyre, S., and Bastviken, D.: Climate-sensitive northern lakes and ponds are critical components of methane release, Nat. Geosci., 9, 99–105, 2016.

USACE.: Method to Estimate River Ice Thickness Based on Meteorological Cold Regions Research and Engineering Laboratory Data Report, 6 pp., U.S. Army Corps of Eng., Hanover, N. H, 2004.

Zhan, P., Song, C., Liu, K., Chen, T., Ke, L., Luo, S., and Fan, C.: Can we estimate the lake mean depth and volume from the deepest record and auxiliary geospatial parameters?, Journal of Hydrology, 617(A), 2023.

Zhuang, Q., Guo, M., Melack, J. M., Lan, X., Tan, Z., Oh, Y., and Leung, L. R.: Current and Future Global Lake Methane Emissions: A Process-Based Modeling Analysis, Journal of Geophysical Research: Biogeosciences, 128, 3, 2023.